Letter

Low temperature phase transitions inside the CDW phase in the kagome metals AV_3Sb_5 (A = Cs, Rb, K): Significance of mixed-type Fermi surface electron correlations

Jianxin Huang,[1] Rina Tazai,[2] Youichi Yamakawa,[1] Seiichiro Onari,[1] and Hiroshi Kontani[1]
[1]*Department of Physics, Nagoya University, Nagoya 464-8602, Japan*
[2]*Yukawa Institute for Theoretical Physics, Kyoto University, Kyoto 606-8502, Japan*

(Received 11 June 2023; accepted 5 January 2024; published 25 January 2024)

To understand the multistage phase transitions in V-based kagome metals inside the charge-density-wave (CDW) phase, we focus on the impact of the "mixed-type" Fermi surface because it is intact in the CDW state on the "pure-type" Fermi surface. On the mixed-type Fermi surface, moderate spin correlations develop, and we reveal that uniform ($\boldsymbol{q} = \boldsymbol{0}$) bond order is caused by the paramagnon interference mechanism, which is described by the Aslamazov-Larkin vertex correction. A dominant solution is E_{2g}-symmetry nematic order, in which the director can be rotated arbitrarily. In addition, we obtain A_{1g}-symmetry order, which leads to the change in the lattice constants without symmetry breaking. The predicted E_{2g} and A_{1g} channel fluctuations at $\boldsymbol{q} = \boldsymbol{0}$ can be observed by the elastoresistance measurements. These results are useful to understand the multistage phase transitions inside the 2×2 CDW phase. The present theory has a general significance because mixed-type Fermi surfaces (with multiorbital van Hove singularities) exist in various kagome lattice systems.

DOI: 10.1103/PhysRevB.109.L041110

Introduction. Exotic electronic states and correlation-driven superconductivity in kagome metals AV_3Sb_5 (A = K, Cs, and Rb) have attracted increasing attention. The strong Coulomb interaction and the geometrical frustration of V site electrons [in Fig. 1(a)] give rise to exotic quantum phase transitions without magnetization. At ambient pressure ($P = 0$), AV_3Sb_5 exhibits 2×2 bond order (BO) at $T_{\rm BO} = 78$, 94, and 102 K for A = K, Cs, and Rb, respectively [1–5]. The BO is the correlation-driven modulation of the hopping integrals (δt_{ij}) [Fig. 1(b)]. The superconducting (SC) state appears at $T_c = 1$–3 K inside the BO phase [6,7]. Under pressure, $T_{\rm BO}$ gradually decreases, while T_c exhibits a non-monotonic pressure dependence [8]. A maximum T_c ($\sim$10 K) is realized around the BO critical pressure $P_c^{\rm BO} \approx 2$ GPa, consistent with the BO fluctuation pairing mechanism proposed in Ref. [9]. The predicted s-wave superconductivity has been recently confirmed by penetration depth and electron irradiation measurements [10,11].

Rich symmetry-breaking states "inside the BO phase" have been a significant open problem. For example, a C_6 symmetry-breaking nematic state [12,13] and time-reversal-symmetry breaking (TRSB) without spin order [4,14–18] have been reported. These states are caused by correlation-driven hopping integral modulation, δt_{ij}. Nematic order is given by the bond order with real δt_{ij}, and TRSB order is given by imaginary δt_{ij}. The latter accompanies a topological charge current [19] that gives the giant anomalous Hall effect (AHE) [20,21]. Theoretically, a sizable off-site (beyond-mean-field) interaction [9,22–46] leads to nonlocal order parameters ($\delta t_{ij} \neq 0$) in kagome metals.

At present, the possible onset temperatures of symmetry-breaking states inside the BO phase are unsolved. One possible state, the TRSB order parameter, strongly develops below $T^* = 35$–50 K in muon spin relaxation/rotation (μSR) [14,16–18] and AHE [20,21] measurements. As for another possibility, the nematic state, a scanning birefringence study [13] reports $T_{\rm nem} \approx T_{\rm BO}$, while $T_{\rm nem} \approx 35$ K is reported by an elastoresistance measurement [12]. This discrepancy may indicate that the BO layer stacking with a π shift leads to weak nematicity at $T_{\rm BO}$, and another nematic order emerges inside the BO phase. The origin of the latter nematicity is not understood at present.

In V-based kagome metals, two major Fermi surfaces (FSs) are composed of b_{3g} orbitals and b_{2g} orbitals [Fig. 1(a)]. The band structure and the FSs are shown in Figs. 1(c) and 1(d), respectively. Both FSs give a large density of states (DOS) at the Fermi level due to the van Hove singularity (vHS) at the three M points. Near the Fermi level, the b_{3g}-orbital FS is called a "pure-type FS," where each vHS point is composed of a single sublattice; see Fig. 1(e). The vHS points are gapped by the 2×2 BO on the pure FS below $T_{\rm BO}$; see the unfolded FS in Fig. 1(d). Previous theories have been devoted mainly to understanding the significant roles of the pure-type FS [9,35–37] except for Refs. [41,43]. However, one may expect that an additional phase transition below $T_{\rm BO}$ would occur on the b_{2g}-orbital FS, a mixed-type FS, because it is not harmed by the BO. Its sublattice weight is shown in Fig. 1(f). In addition, it is notable that a mixed-type FS universally exists in the usual kagome lattice models. Therefore, the research on the mixed-type FS is of great significance.

In this Letter, to understand the phase transitions below $T_{\rm BO}$ in AV_3Sb_5, we focus on the impact of the mixed-type FS because it is intact in the BO phase. On the mixed-type FS, moderate antiferromagnetic (AFM) spin correlations develop, which lead to the uniform ($\boldsymbol{q} = \boldsymbol{0}$) bond order by the paramagnon interference mechanism. This beyond-mean-field mechanism is described by the Aslamazov-Larkin (AL) vertex corrections. A dominant BO solution is the E_{2g}-symmetry

 ©2024 American Physical Society

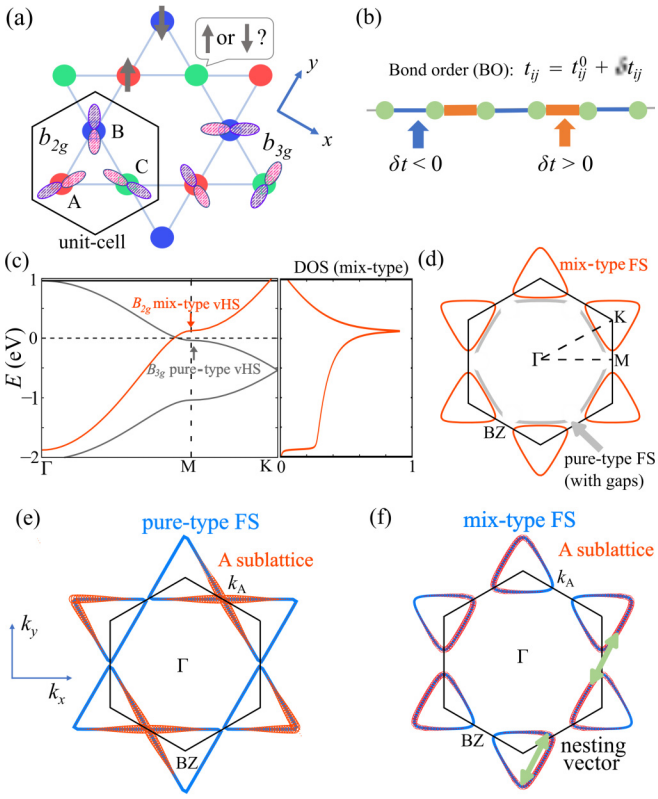

FIG. 1. (a) Kagome lattice structure. b_{3g} and b_{2g} orbitals are shown. (b) The BO parameter given by the hopping integral modulation δt_{ij}. (c) b_{3g}-orbital (with pure-type vHS) and b_{2g}-orbital (with mixed-type vHS) band structures with the DOS. (d) FSs of pure-type FS ($n^{\rm pure} = 2.6$) and mixed-type FS ($n^{\rm mix} = 1.6$). Here, the pure-type FS exhibits a 2×2 BO-induced gap. (e) A-sublattice weight shown by the red color on the pure-type FS at $n^{\rm pure}_{\rm vHF} = 2.5$. The vHS point at $\boldsymbol{k} = \boldsymbol{k}_{\rm A}$ is composed of the A sublattice. (f) A-sublattice weight on the mixed-type FS at $n^{\rm mix}_{\rm vHF} = 1.6$. The vHS point at $\boldsymbol{k} = \boldsymbol{k}_{\rm A}$ is composed of B+C sublattices.

nematic order in which the director can be rotated arbitrarily. In addition, we obtain the A_{1g}-symmetry bond order which would accompany the change in the lattice constants. These results are useful to understand the multistage phase transitions inside the 2×2 BO phase.

Model Hamiltonian and formulations. In this Letter, we study the bond-order phase transition mediated by the quantum fluctuations in a kagome lattice Hubbard model with a mixed-type FS composed of three b_{2g} orbitals. We apply the density-wave (DW) equation method to derive the optimized order parameter (=symmetry-breaking self-energy $\Delta\Sigma$) driven by the beyond-mean-field vertex corrections. In Ref. [9], the present authors studied the $b_{2g} + b_{3g}$ orbital kagome lattice Hubbard model for AV_3Sb_5, and found that the pure-type FS alone gives the 2×2 BO state. However, the b_{2g}-orbital FS can induce different instabilities for $T \ll T_{\rm BO}$. For this reason, to find the phase transition inside the BO phase, we study the b_{2g}-orbital kagome lattice tight-binding Hubbard model.

The b_{2g} orbitals at sublattices A–C are shown in Fig. 1(a). The corresponding mixed-type FS is shown in Fig. 1(d). The kinetic term of the b_{2g}-orbital model is

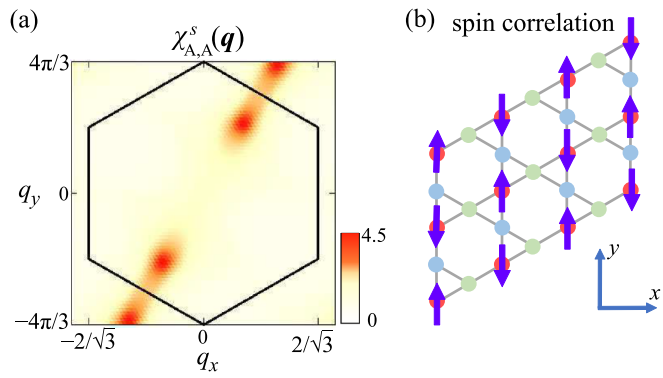

FIG. 2. (a) Obtained $\chi^s_{\rm A,A}(\boldsymbol{q})$ that shows the AFM correlation. (b) Real-space short-range spin correlation.

$H_0 = \sum_{\boldsymbol{k},l,m,\sigma} h_{lm}(\boldsymbol{k}) c^\dagger_{\boldsymbol{k},l,\sigma} c_{\boldsymbol{k},m,\sigma}$, where $h_{lm}(\boldsymbol{k})$ is the momentum representation of the nearest-neighbor hopping integral $t_{lm}(r)$, $l, m =$ A, B, C and σ is the spin index. In our study the unit of energy (Coulomb interaction, hopping integral, and temperature) is eV. We set the nearest-neighbor hopping integral $t = -0.5$ [9,35] and put the number of electrons on the mixed-type FS $n^{\rm mix} = 1.6$. The 3×3 Green's function is given as $\hat{G}(\boldsymbol{k}, \epsilon_n) = [(i\epsilon_n + \mu)\hat{1} - \hat{h}(\boldsymbol{k})]^{-1}$, where $\epsilon_n = (2n + 1)\pi T$ is the fermion Matsubara frequency. We also introduce the on-site Coulomb interaction term $H_U = U \sum_{i,l} n_{i,l,\uparrow} n_{i,l,\downarrow}$, where $n_{i,l,\sigma}$ is the electron number at unit cell i.

In the mean-field-level approximation, the spin instability is the most prominent [9]. In the random phase approximation (RPA), the spin susceptibility is $\hat{\chi}^s(q) = \hat{\chi}^0(q)[\hat{1} - U\hat{\chi}^0(q)]^{-1}$, where $\chi^0_{l,m}(q) = -T \sum_k G_{l,m}(k+q) G_{m,l}(k)$ is the 3×3 irreducible susceptibility matrix and $q \equiv (\boldsymbol{q}, \omega_l = 2\pi T l)$. The spin susceptibility diverges when the spin Stoner factor α_s, which is defined as the maximum eigenvalue of $U\hat{\chi}^0(q)$, reaches unity. Figure 2(a) shows the spin susceptibility $\chi^s_{\rm A,A}(\boldsymbol{q})$ at $T = 0.02$ and $\alpha_s = 0.97$ ($U = 2.2$). Its maximum peak appears at the nesting of the A-sublattice FS shown in Fig. 1(f). The real-space short-range spin correlation is depicted in Fig. 2(b). In contrast, such AFM spin fluctuations remain small in the pure-type case. The obtained $\chi^s(\boldsymbol{q})$ is used to construct the kernel function of the DW equation, $I^{L,M}_q(k, p)$ in Eq. (1), which is a nonlinear function of $\chi^s(\boldsymbol{q})$. We will show that the AFM spin fluctuations in the mixed-type FS give rise to the exotic ferro-bond order via the AL vertex corrections.

Density-wave equation analysis. The nonmagnetic DW orders cannot be obtained by RPA in the Hubbard model with the on-site Coulomb interaction, because the charge Stoner factor α_c is always smaller than the spin Stoner factor α_s in the mean-field approximation. However, the vertex corrections in the DW equation [Fig. 3(a)] give various charge-channel DW states due to the paramagnon interference processes.

From a field-theoretical point of view, the nonmagnetic bond order is described as the symmetry-breaking self-energy $\Delta\Sigma$, which is simply the DW order parameter [30]. ($\Delta\Sigma$ is much smaller than the self-energy without symmetry breaking Σ_0.) Once $\Delta\Sigma$ emerges, it will give the symmetry breaking in $\chi^0(q) = -T \sum_k G(k+q) G(k)$, where G is the Green's function with the total self-energy $\Sigma_{\rm tot}(k) = \Delta\Sigma(k) + \Sigma_0(k)$.

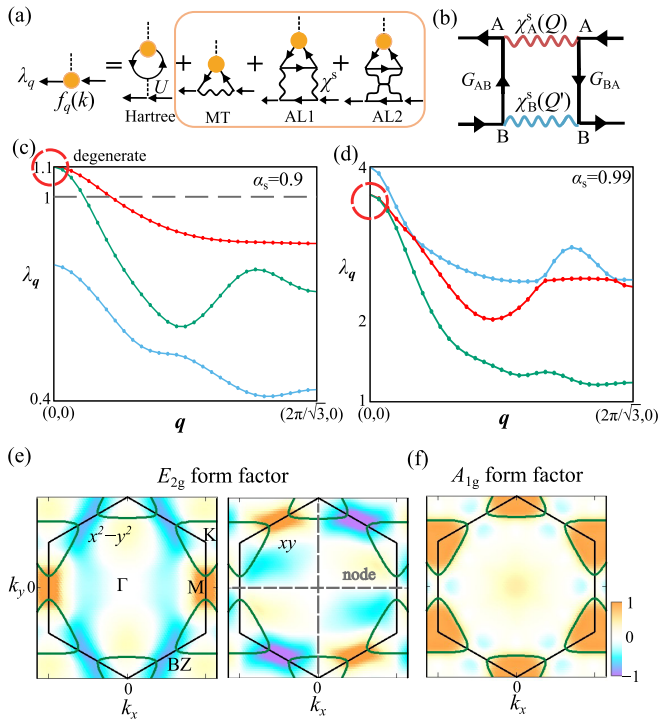

FIG. 3. (a) Linearized DW equation with respect to the form factor $f_{\boldsymbol{q}}(k)$ and eigenvalue $\lambda_{\boldsymbol{q}}$. The p-h pairing interaction is composed of the Hartree term, the MT term, and the AL terms. The solid line is the noninteracting Green's function, and the wavy lines are the spin fluctuations from RPA. (b) Interference between two paramagnons ($\boldsymbol{Q}$ and $\boldsymbol{Q}'$) that leads to the DW order at $\boldsymbol{q} = \boldsymbol{Q} - \boldsymbol{Q}'$. (c), (d) Eigenvalue $\lambda_{\boldsymbol{q}}$ for two cases: (c) Moderate ($\alpha_S = 0.9$) and (d) strong ($\alpha_S = 0.99$) spin fluctuation. Three states are shown in different colors. In both cases, $\lambda_{\boldsymbol{q}}$ exhibits the maximum at $\boldsymbol{q} = \boldsymbol{0}$. (e), (f) Diagonal form factor $\sum_l^{\mathrm{A,B,C}} f^{ll}_{\boldsymbol{q}=\boldsymbol{0}}(k)$: (e) E_{2g}-symmetry solution obtained for $\alpha_S = 0.9$ and (f) A_{1g}-symmetry solution obtained for $\alpha_S = 0.99$. Note that the off-diagonal form factor is also large.

In the meanwhile, when symmetry breaking in $\chi^s(\boldsymbol{q})$ emerges, the self-energy $\Sigma(k) = \frac{3U^2}{2} T \sum_q \chi^s(q) G(k+q)$ will contain finite $\Delta\Sigma = \Sigma(k) - \Sigma_0(k)$. Such feedback between $\Delta\Sigma$ and $\chi^s(\boldsymbol{q})$ becomes positive when $\lambda > 1$, so the nonmagnetic bond order occurs spontaneously. In the DW equation, the form factor describes $\Delta\Sigma$, and the AL terms give the positive feedback effect [47]. This theory was first developed to explain the orbital nematic state in Fe-based superconductors, and it has been applied successfully to the cuprates and the twisted-bilayer graphene [30]. Recently, the BO and current ordered states in kagome metals with the pure-type FS also have been explained by the AL processes [9,38].

The DW equation for the charge-channel order is

$$\lambda_{\boldsymbol{q}} f^L_{\boldsymbol{q}}(k) = -\frac{T}{N} \sum_{p, M_1, M_2} I^{L,M_1}_{\boldsymbol{q}}(k,p) \times \{G(p)G(p+\boldsymbol{q})\}^{M_1,M_2} f^{M_2}_{\boldsymbol{q}}(p), \quad (1)$$

where $I^{L,M}_{\boldsymbol{q}}(k,p)$ is the particle-hole (p-h) pairing interaction, the kernel function for the charge channel. The details of this are given in the Supplemental Material (SM) A [48]. $k \equiv (\boldsymbol{k}, \epsilon_n)$ and $p \equiv (\boldsymbol{p}, \epsilon_m)$ (ϵ_n, ϵ_m are fermion Matsubara frequencies). $L \equiv (l, l')$ and $M_i \equiv (m_i, m_i')$ represent the pair of sublattice indices A, B, C. $\lambda_{\boldsymbol{q}}$ is the eigenvalue that represents the instability of the DW at wave vector $\boldsymbol{q}$, and $\max_{\boldsymbol{q}}\{\lambda_{\boldsymbol{q}}\}$ reaches unity at $T = T_{\mathrm{DW}}$. $f^L_{\boldsymbol{q}}(k)$ is the Hermitian form factor that is proportional to the p-h condensation $\sum_\sigma \{\langle c^\dagger_{\boldsymbol{k}+\boldsymbol{q},l,\sigma} c_{\boldsymbol{k},l',\sigma}\rangle - \langle\cdots\rangle_0\}$, or equivalently, the symmetry-breaking self-energy $\Delta\Sigma$. In real space, the $\boldsymbol{k}$-dependent form factor gives the correlated hopping between (i,l) and (j,m), which is given as $\delta t_{il,jm} (= \delta t_{jm,il})^*$,

$$\delta t_{il,jm} = \frac{1}{N} \sum_{\boldsymbol{k}} f^{lm}_{\boldsymbol{q}}(\boldsymbol{k}) e^{i\boldsymbol{k}\cdot(\boldsymbol{r}_{il} - \boldsymbol{r}_{jm})} e^{i\boldsymbol{q}\cdot\boldsymbol{r}_{il}}, \quad (2)$$

where $\boldsymbol{r}_{il}$ represents the position of the l sublattice in the unit cell i. The BO preserves the time-reversal symmetry: $\delta t_{il,jm} = \delta t_{jm,il} = $ real.

The kernel function $I^{L,M}_{\boldsymbol{q}}$ is given by the functional derivative of the Luttinger-Ward function $\Phi_{\mathrm{LW}}(G)$. Here, we apply the fluctuation-exchange approximation for $\Phi_{\mathrm{LW}}(G)$. Then, $I^{L,M}_{\boldsymbol{q}}$ is composed of one Hartree term, one single-magnon exchange Maki-Thompson (MT) term, and two double-magnon interference Aslamazov-Larkin (AL) terms, as depicted in Fig. 3(a) [30]. Importantly, the AL terms represent the interference between two paramagnons with momenta $\boldsymbol{Q}$ and $\boldsymbol{Q}'$ that leads to the DW order at $\boldsymbol{q} = \boldsymbol{Q} - \boldsymbol{Q}'$; see Fig. 3(b).

With the obtained spin susceptibility as the paramagnon, we solve the DW equation. The $\boldsymbol{q}$ dependence of the eigenvalue $\lambda_{\boldsymbol{q}}$ at $n^{\mathrm{mix}} = 1.6$ ($T = 0.02$) is exhibited in Figs. 3(c) and 3(d). (Here, we show $\lambda_{\boldsymbol{q}}$ only on the path Γ-M because $\lambda_{\boldsymbol{q}}$ on the path M-K-Γ is small.) Figure 3(c) [Fig. 3(d)] shows the result for $\alpha_s = 0.9$ (0.99), where the spin fluctuation strength is moderate (strong). Importantly, the maximum peak position is located at $\boldsymbol{q} = \boldsymbol{0}$ in both cases. The obtained $\boldsymbol{q} = \boldsymbol{0}$ order, which is very different from the nesting driven $\boldsymbol{q} \neq \boldsymbol{0}$ order, is naturally derived from the interference between two paramagnons with wave vectors $\boldsymbol{Q}$ and $\boldsymbol{Q}'(= \boldsymbol{Q})$ [30]. For $\alpha_S = 0.9$ in Fig. 3(c), the largest two eigenvalues are degenerate, and the corresponding form factors are E_{2g}-symmetry BOs $[\hat{f}_{x^2-y^2}(k), \hat{f}_{xy}(k)]$. The corresponding diagonal form factor $\sum_l f^{ll}_{\boldsymbol{q}=\boldsymbol{0}}(k)$ is shown in Fig. 3(e). Note that off-diagonal form factors are as large as the diagonal form factors. For $\alpha_S = 0.99$ in Fig. 3(d), the nondegenerate largest eigenvalue corresponds to the A_{1g}-symmetry form factor shown in Fig. 3(f).

The E_{2g}-symmetry BO gives the nematicity, and its director can be rotated at any angle by taking the linear combination of $\hat{f}_{x^2-y^2}(k)$ and $\hat{f}_{xy}(k)$ [25]. To understand the nature of the E_{2g}-symmetry nematic state, we discuss the real-space form factor $\delta t_{il,jm}$ based on Eq. (2). When the wave vector is $\boldsymbol{q} = \boldsymbol{0}$, $\delta t_{il,jm}$ is simply written as $\delta t_{lm}(\boldsymbol{r})$ with $\boldsymbol{r} \equiv \boldsymbol{r}_{il} - \boldsymbol{r}_{jm}$. The obtained $\delta t_{lm}(\boldsymbol{r})$ for $f^{lm}_{x^2-y^2}(k)$ at $\boldsymbol{q} = \boldsymbol{0}$ is shown in Fig. 4(a). [Its schematic picture is given in Fig. 4(b).] It is plotted in two directions (AB and AC) from sublattice A, as a function of the distance R, where the distance between nearest sites is 1. The BO along the BC direction is the same as that along the AC direction. [The even-parity relation $\delta t_{lm}(R) = \delta t_{ml}(-R)$ is verified.] δt_{ll} at $R = 0$ represents the on-site charge modulation at sublattice l, and δt_{lm} at $R = \pm 1$ ($l \neq m$) represents BO between the nearest sites.

A schematic picture of the hopping modulation due to the nearest BO is given in Fig. 4(c). In this case, the

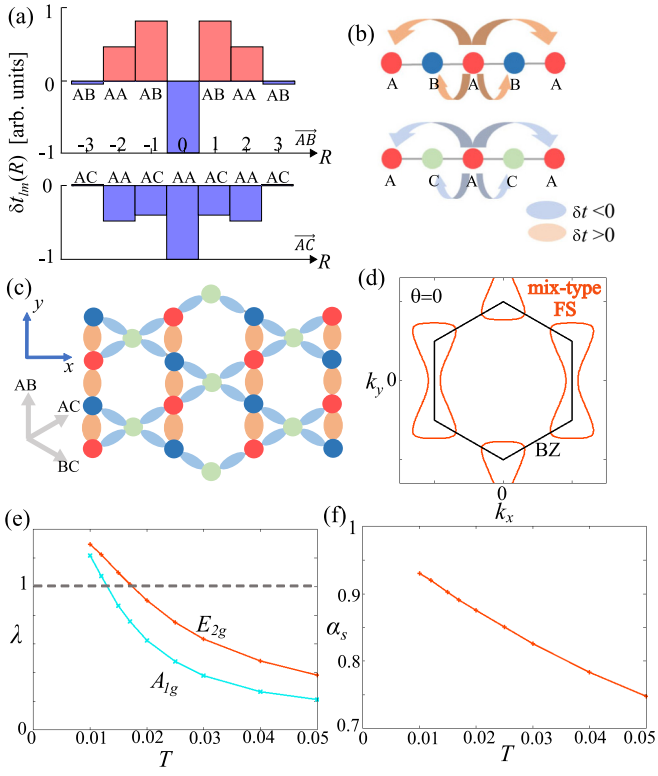

FIG. 4. (a) Obtained $\delta t_{lm}(R)$ along two directions. The horizontal axis means the real-space distance. For example, in the AB direction, $R = 1$ (2) marks the hopping modulation between the nearest A and B (A and A). Note that $\delta t_{\rm AC}(R) = \delta t_{\rm BC}(R)$. (b) Schematic pictures of $\delta t_{lm}(R)$. (c) Nematic bond order in real space for $\hat{f}_{x^2-y^2}$. The orange color represents $\delta t_{ij} > 0$, while the blue color represents $\delta t_{ij} < 0$. (d) Nematic FS induced by the nematic BO $\hat{f}_\theta$. It can be rotated to any angle by changing the angle θ. (e) T dependence of $\lambda_{\boldsymbol{q}=\boldsymbol{0}}$ for E_{2g} and A_{1g} states, for $U = 1.95$. (f) T dependence of α_S.

lattice structure will become nematic in the presence of finite electron-phonon coupling due to the E_{2g} acoustic mode. We also discuss the FS deformation due to the E_{2g} nematic BO, under the order parameter $H' = \Delta E \sum_{\boldsymbol{k}\sigma} \hat{c}^\dagger_{\boldsymbol{k}\sigma} \hat{f}_\theta(\boldsymbol{k}) \hat{c}_{\boldsymbol{k}\sigma}$, where $\hat{f}_\theta(\boldsymbol{k}) \equiv \cos\theta \hat{f}_{x^2-y^2}(\boldsymbol{k}) + \sin\theta \hat{f}_{xy}(\boldsymbol{k})$. The ordered nematic FS at $\theta = 0$ with $\Delta E = 0.01$ is showed in Fig. 4(d). By changing the angle θ, the nematic FS can be rotated to any direction.

Another state, the A_{1g} BO, does not break the symmetry of the system. However, it induces the FS deformation due to the hopping modulation and the change in the lattice constants should be accompanied through the finite electron-phonon coupling. In SM B [48], we present the nontrivial hopping modulation caused by the A_{1g} BO.

Figure 4(e) shows the T dependence of λ for the E_{2g} and A_{1g} states, in the case of $U = 1.95$. The obtained λ monotonically increases with decreasing T, while the increment of α_S is moderate [see Fig. 4(f)]. Although the obtained transition temperature is relatively high, it will be reduced to below $T_{\rm BO}$ by introducing the self-energy effect [47]. In fact, due to the ordinary self-energy Σ_0 which breaks no symmetry, the Green's function is given as $G = 1/(i\epsilon_n - \Sigma_0 - \epsilon_k) \approx z/(i\epsilon_n - z\epsilon_k)$, where the mass-enhancement factor $z^{-1} = m^*/m$ is larger than 1. The factor z leads to the rescaling, $T \to zT$ and $U \to U/z$, under the condition of fixed α and λ [23]. Thus, the transition temperature will be reduced by z. It is an important future issue to derive a reliable transition temperature by taking account the self-energy.

In SM C [48], we discuss the important roles of the AL and MT vertex corrections for the BO. We show that the AL term gives a large positive contribution for both E_{2g} and A_{1g} BOs. In addition, it is found that the MT term slightly favors the nodal A_{1g} BO. Interestingly, the same AL process leads to the $\boldsymbol{q} = \boldsymbol{0}$ BO in the mixed-type FS model and 2×2 BO in the pure-type FS model.

Finally, we discuss the results of the existing elastoresistance experiments [49–51] based on the present theory. In Ref. [49], a significant E_{2g} symmetry channel nematic correlation is observed under $T_{\rm CDW}$ and above a transition temperature $T_{\rm nem} \sim 35$ K. In contrast, in other experiments [50,51], a strong enhancement of the A_{1g} channel susceptibility is reported below $T_{\rm CDW}$ and presents a phase transition at $T^* \sim 20$ K. Importantly, both E_{2g} and A_{1g} instabilities develop in the mixed-type FS in the present theory, and the leading instability can exchange. Thus, different experimental results may originate from a slight sample dependence. Noteworthy, Ref. [52] reports the nematic order is strongly stabilized under tiny (extrinsic) strain in a kagome metal. Thus, the DW equation analysis for the distorted kagome metal model would be useful to understand the variety of the experimental reports. This is an important future issue.

Summary. We studied the phase transitions below $T_{\rm BO}$ in AV_3Sb_5 by focusing on the mixed-type FS that is intact in the BO phase. It is revealed that the paramagnon interference mechanism leads to uniform ($\boldsymbol{q} = \boldsymbol{0}$) bond order. A dominant solution is the E_{2g}-symmetry nematic order. We also obtain the A_{1g}-symmetry non-nematic order. These results are useful to understand the multistage phase transitions inside the 2×2 BO phase. This theory has general significance because mixed types like multisublattice FS exist in many kagome metals, such as ATi_3Bi_5 [53]. In this case, the intrasublattice nesting gives rise to the AFM spin correlation and such correlation leads to paramagnon interference. Thus, due to this mechanism, exotic bond orders would occur in various kagome metals.

Acknowledgments. This study has been supported by Grants-in-Aid for Scientific Research from Ministry of Education, Culture, Sports, Science and Technology of Japan (Grants No. JP18H01175, No. JP20K03858, No. JP20K22328, No. JP22K14003, and No. JP23K03299), and by the Quantum Liquid Crystal No. JP19H05825 KAKENHI on Innovative Areas from Japan Society for the promotion of Science of Japan.

[1] B. R. Ortiz, L. C. Gomes, J. R. Morey, M. Winiarski, M. Bordelon, J. S. Mangum, I. W. H. Oswald, J. A. Rodriguez-Rivera, J. R. Neilson, S. D. Wilson, E. Ertekin, T. M. McQueen, and E. S. Toberer, New kagome prototype materials:

Discovery of KV_3Sb_5, RbV_3Sb_5, and CsV_3Sb_5, Phys. Rev. Mater. **3**, 094407 (2019).

[2] B. R. Ortiz, S. M. L. Teicher, Y. Hu, J. L. Zuo, P. M. Sarte, E. C. Schueller, A. M. M. Abeykoon, M. J. Krogstad, S. Rosenkranz, R. Osborn, R. Seshadri, L. Balents, J. He, and S. D. Wilson, CsV_3Sb_5: A $\mathbb{Z}_2$ topological kagome metal with a superconducting ground state, Phys. Rev. Lett. **125**, 247002 (2020).

[3] C. Mu, Q. Yin, Z. Tu, C. Gong, H. Lei, Z. Li, and J. Luo, S-wave superconductivity in kagome metal CsV_3Sb_5 revealed by $^{121/123}$Sb NQR and ^{51}V NMR measurements, Chin. Phys. Lett. **38**, 077402 (2021).

[4] Y.-X. Jiang, J.-X. Yin, M. M. Denner, N. Shumiya, B. R. Ortiz, G. Xu, Z. Guguchia, J. He, M. S. Hossain, X. Liu, J. Ruff, L. Kautzsch, S. S. Zhang, G. Chang, I. Belopolski, Q. Zhang, T. A. Cochran, D. Multer, M. Litskevich, Z.-J. Cheng *et al.*, Unconventional chiral charge order in kagome superconductor KV_3Sb_5, Nat. Mater. **20**, 1353 (2021).

[5] H. Li, H. Zhao, B. R. Ortiz, T. Park, M. Ye, L. Balents, Z. Wang, S. D. Wilson, and I. Zeljkovic, Rotation symmetry breaking in the normal state of a kagome superconductor KV_3Sb_5, Nat. Phys. **18**, 265 (2022).

[6] B. R. Ortiz, P. M. Sarte, E. M. Kenney, M. J. Graf, S. M. L. Teicher, R. Seshadri, and S. D. Wilson, Superconductivity in the $\mathbb{Z}_2$ kagome metal KV_3Sb_5, Phys. Rev. Mater. **5**, 034801 (2021).

[7] Q. Yin, Z. Tu, C. Gong, Y. Fu, S. Yan, and H. Lei, Superconductivity and normal-state properties of kagome metal RbV_3Sb_5 single crystals, Chin. Phys. Lett. **38**, 037403 (2021).

[8] F. H. Yu, D. H. Ma, W. Z. Zhuo, S. Q. Liu, X. K. Wen, B. Lei, J. J. Ying, and X. H. Chen, Unusual competition of superconductivity and charge-density-wave state in a compressed topological kagome metal, Nat. Commun. **12**, 3645 (2021).

[9] R. Tazai, Y. Yamakawa, S. Onari, and H. Kontani, Mechanism of exotic density-wave and beyond-Migdal unconventional superconductivity in kagome metal AV_3Sb_5 (A = K, Rb, Cs), Sci. Adv. **8**, eabl4108 (2022).

[10] M. Roppongi, K. Ishihara, Y. Tanaka, K. Ogawa, K. Okada, S. Liu, K. Mukasa, Y. Mizukami, Y. Uwatoko, R. Grasset, M. Konczykowski, B. R. Ortiz, S. D. Wilson, K. Hashimoto, and T. Shibauchi, Bulk evidence of anisotropic *s*-wave pairing with no sign change in the kagome superconductor CsV_3Sb_5, Nat. Commun. **14**, 667 (2023).

[11] W. Zhang, X. Liu, L. Wang, C. W. Tsang, Z. Wang, S. T. Lam, W. Wang, J. Xie, X. Zhou, Y. Zhao, S. Wang, J. Tallon, K. T. Lai, and S. K. Goh, Nodeless superconductivity in kagome metal CsV_3Sb_5 with and without time reversal symmetry breaking, Nano Lett. **23**, 872 (2023).

[12] L. Nie, K. Sun, W. Ma, D. Song, L. Zheng, Z. Liang, P. Wu, F. Yu, J. Li, M. Shan, D. Zhao, S. Li, B. Kang, Z. Wu, Y. Zhou, K. Liu, Z. Xiang, J. Ying, Z. Wang, T. Wu *et al.*, Charge-density-wave-driven electronic nematicity in a kagome superconductor, Nature (London) **604**, 59 (2022).

[13] Y. Xu, Z. Ni, Y. Liu, B. R. Ortiz, Q. Deng, S. D. Wilson, B. Yan, L. Balents, and L. Wu, Three-state nematicity and magneto-optical Kerr effect in the charge density waves in kagome superconductors, Nat. Phys. **18**, 1470 (2022).

[14] L. Yu, C. Wang, Y. Zhang, M. Sander, S. Ni, Z. Lu, S. Ma, Z. Wang, Z. Zhao, H. Chen, K. Jiang, Y. Zhang, H. Yang, F. Zhou, X. Dong, S. L. Johnson, M. J. Graf, J. Hu, H.-J. Gao, and Z. Zhao, Evidence of a hidden flux phase in the topological kagome metal CsV_3Sb_5, arXiv:2107.10714.

[15] C. Mielke III, D. Das, J.-X. Yin, H. Liu, R. Gupta, Y.-X. Jiang, M. Medarde, X. Wu, H. C. Lei, J. Chang, P. Dai, Q. Si, H. Miao, R. Thomale, T. Neupert, Y. Shi, R. Khasanov, M. Z. Hasan, H. Luetkens, and Z. Guguchia, Time-reversal symmetry-breaking charge order in a kagome superconductor, Nature (London) **602**, 245 (2022).

[16] R. Khasanov, D. Das, R. Gupta, C. Mielke, M. Elender, Q. Yin, Z. Tu, C. Gong, H. Lei, E. T. Ritz, R. M. Fernandes, T. Birol, Z. Guguchia, and H. Luetkens, Time-reversal symmetry broken by charge order in CsV_3Sb_5, Phys. Rev. Res. **4**, 023244 (2022).

[17] Z. Guguchia, C. Mielke III, D. Das, R. Gupta, J.-X. Yin, H. Liu, Q. Yin, M. H. Christensen, Z. Tu, C. Gong, N. Shumiya, M. S. Hossain, T. Gamsakhurdashvili, M. Elender, P. Dai, A. Amato, Y. Shi, H. C. Lei, R. M. Fernandes, M. Z. Hasan *et al.*, Tunable unconventional kagome superconductivity in charge ordered RbV_3Sb_5 and KV_3Sb_5, Nat. Commun. **14**, 153 (2023).

[18] C. Guo, C. Putzke, S. Konyzheva, X. Huang, M. Gutierrez-Amigo, I. Errea, D. Chen, M. G. Vergniory, C. Felser, M. H. Fischer, T. Neupert, and P. J. W. Moll, Switchable chiral transport in charge-ordered kagome metal CsV_3Sb_5, Nature (London) **611**, 461 (2022).

[19] F. D. M. Haldane, Model for a quantum Hall effect without Landau levels: Condensed-matter realization of the "parity anomaly", Phys. Rev. Lett. **61**, 2015 (1988).

[20] S.-Y. Yang, Y. Wang, B. R. Ortiz, D. Liu, J. Gayles, E. Derunova, R. Gonzalez-Hernandez, L. Šmejkal, Y. Chen, S. S. P. Parkin, S. D. Wilson, E. S. Toberer, T. McQueen, and M. N. Ali, Giant, unconventional anomalous Hall effect in the metallic frustrated magnet candidate, KV_3Sb_5, Sci. Adv. **6**, eabb6003 (2020).

[21] F. H. Yu, T. Wu, Z. Y. Wang, B. Lei, W. Z. Zhuo, J. J. Ying, and X. H. Chen, Concurrence of anomalous Hall effect and charge density wave in a superconducting topological kagome metal, Phys. Rev. B **104**, L041103 (2021).

[22] S. Onari and H. Kontani, Self-consistent vertex correction analysis for iron-based superconductors: Mechanism of Coulomb interaction-driven orbital fluctuations, Phys. Rev. Lett. **109**, 137001 (2012).

[23] Y. Yamakawa, S. Onari, and H. Kontani, Nematicity and magnetism in FeSe and other families of Fe-based superconductors, Phys. Rev. X **6**, 021032 (2016).

[24] S. Onari, Y. Yamakawa, and H. Kontani, Sign-reversing orbital polarization in the nematic phase of FeSe due to the C_2 symmetry-breaking in the self-energy, Phys. Rev. Lett. **116**, 227001 (2016).

[25] S. Onari and H. Kontani, SU(4) valley + spin fluctuation interference mechanism for nematic order in magic-angle twisted bilayer graphene: The impact of vertex corrections, Phys. Rev. Lett. **128**, 066401 (2022).

[26] M. Tsuchiizu, Y. Ohno, S. Onari, and H. Kontani, Orbital nematic instability in the two-orbital Hubbard model: Renormalization-group+constrained RPA analysis, Phys. Rev. Lett. **111**, 057003 (2013).

[27] M. Tsuchiizu, K. Kawaguchi, Y. Yamakawa, and H. Kontani, Multistage electronic nematic transitions in cuprate superconductors: A functional-renormalization-group analysis, Phys. Rev. B **97**, 165131 (2018).

[28] A. V. Chubukov, M. Khodas, and R. M. Fernandes, Magnetism, superconductivity, and spontaneous orbital order in iron-based

superconductors: Which comes first and why? Phys. Rev. X **6**, 041045 (2016).

[29] R. M. Fernandes, P. P. Orth, and J. Schmalian, Intertwined vestigial order in quantum materials: Nematicity and beyond, Annu. Rev. Condens. Matter Phys. **10**, 133 (2019).

[30] H. Kontani, R. Tazai, Y. Yamakawa, and S. Onari, Unconventional density waves and superconductivities in Fe-based superconductors and other strongly correlated electron systems, Adv. Phys. **70**, 355 (2021).

[31] R. Tazai, Y. Yamakawa, M. Tsuchiizu, and H. Kontani, d- and p-wave quantum liquid crystal orders in cuprate superconductors, κ-(BEDT-TTF)$_2$X, and coupled chain Hubbard models: Functional-renormalization-group analysis, J. Phys. Soc. Jpn. **90**, 111012 (2021).

[32] K. Kawaguchi, Y. Yamakawa, M. Tsuchiizu, and H. Kontani, Competing unconventional charge-density-wave states in cuprate superconductors: Spin-fluctuation-driven mechanism, J. Phys. Soc. Jpn. **86**, 063707 (2017).

[33] Y. Yamakawa and H. Kontani, Spin-fluctuation-driven nematic charge-density-wave in cuprate superconductors: Impact of Aslamazov-Larkin-type vertex correction, Phys. Rev. Lett. **114**, 257001 (2015).

[34] J. C. S. Davis and D.-H. Lee, Concepts relating magnetic interactions, intertwined electronic orders, and strongly correlated superconductivity, Proc. Natl. Acad. Sci. USA **110**, 17623 (2013).

[35] X. Wu, T. Schwemmer, T. Müller, A. Consiglio, G. Sangiovanni, D. Di Sante, Y. Iqbal, W. Hanke, A. P. Schnyder, M. M. Denner, M. H. Fischer, T. Neupert, and R. Thomale, Nature of unconventional pairing in the kagome superconductors AV_3Sb_5 (A = K, Rb, Cs), Phys. Rev. Lett. **127**, 177001 (2021).

[36] M. M. Denner, R. Thomale, and T. Neupert, Analysis of charge order in the kagome metal AV_3Sb_5 (A = K, Rb, Cs), Phys. Rev. Lett. **127**, 217601 (2021).

[37] T. Park, M. Ye, and L. Balents, Electronic instabilities of kagome metals: Saddle points and Landau theory, Phys. Rev. B **104**, 035142 (2021).

[38] R. Tazai, Y. Yamakawa, and H. Kontani, Charge-loop current order and Z_3 nematicity mediated by bond-order fluctuations in kagome metals, Nat. Commun. **14**, 7845 (2023).

[39] R. Tazai, Y. Yamakawa, and H. Kontani, Drastic magnetic-field-induced chiral current order and emergent current-bond-field interplay in kagome metals, Proc. Natl. Acad. Sci. USA **121**, e2303476121 (2024).

[40] T. Schwemmer, H. Hohmann, M. Durrnagel, J. Potten, J. Beyer, S. Rachel, Y.-M. Wu, S. Raghu, T. Müller, W. Hanke *et al.*, Pair density wave instability in the kagome Hubbard model, arXiv:2302.08517.

[41] M. H. Christensen, T. Biro, B. M. Andersen, and R. M. Fernandes, Loop currents in AV_3Sb_5 kagome metals: Multipolar and toroidal magnetic orders, Phys. Rev. B **106**, 144504 (2022).

[42] F. Grandi, A. Consiglio, M. A. Sentef, R. Thomale, and D. M. Kennes, Theory of nematic charge orders in kagome metals, Phys. Rev. B **107**, 155131 (2023).

[43] H. D. Scammell, J. Ingham, T. Li, and O. P. Sushkov, Chiral excitonic order from twofold van Hove singularities in kagome metals, Nat. Commun. **14**, 605 (2023).

[44] A. Ptok, A. Kobialka, M. Sternik, J. Lazewski, P. T. Jochym, A. M. Oles, and P. Piekarz, Dynamical study of the origin of the charge density wave in AV_3Sb_5 (A = K, Rb, Cs) compounds, Phys. Rev. B **105**, 235134 (2022).

[45] H. Kontani, Y. Yamakawa, R. Tazai, and S. Onari, Odd-parity spin-loop-current order mediated by transverse spin fluctuations in cuprates and related electron systems, Phys. Rev. Res. **3**, 013127 (2021).

[46] R. Tazai and H. Kontani, Multipole fluctuation theory for heavy fermion systems: Application to multipole orders in CeB_6, Phys. Rev. B **100**, 241103(R) (2019).

[47] R. Tazai, S. Matsubara, Y. Yamakawa, S. Onari, and H. Kontani, Rigorous formalism for unconventional symmetry breaking in Fermi liquid theory and its application to nematicity in FeSe, Phys. Rev. B **107**, 035137 (2023).

[48] See Supplemental Material at http://link.aps.org/supplemental/10.1103/PhysRevB.109.L041110 for SM A: Formula of DW equation, SMB: A_{1g} mode, SM C: Important roles of the AL and MT vertex corrections and the quantum interference mechanism.

[49] Y. Sur, K. T. Kim, S. Kim, and K. H. Kim, Optimized superconductivity in the vicinity of a nematic quantum critical point in the kagome superconductor $Cs(V_{1-x}Ti_x)_3Sb_5$, Nat. Commun. **14**, 3899 (2023).

[50] Z. Liu, Y. Shi, Q. Jiang, E. W. Rosenberg, J. M. DeStefano, J. Liu, C. Hu, Y. Zhao, Z. Wang, Y. Yao, D. Graf, P. Dai, J. Yang, X. Xu, and J. Chu, Absence of nematic instability in the kagome metal CsV_3Sb_5, arXiv:2309.14574.

[51] T. Asaba, A. Onishi, Y. Kageyama, T. Kiyosue, K. Ohtsuka, S. Suetsugu, Y. Kohsaka, T. Gaggl, Y. Kasahara, H. Murayama, K. Hashimoto, R. Tazai, H. Kontani, B. R. Ortiz, S. D. Wilson, Q. Li, H.-H. Wen, T. Shibauchi, and Y. Matsuda, Evidence for an odd-parity nematic phase above the charge density wave transition in kagome metal CsV_3Sb_5, arXiv:2309.16985.

[52] C. Guo, C. Putzke, S. Konyzheva, X. Huang, M. Gutierrez-Amigo, I. Errea, D. Chen, M. G. Vergniory, C. Felser, M. H. Fischer, T. Neupert, and P. J. W. Moll, Correlated order at the tipping point in the kagome metal CsV_3Sb_5, arXiv:2304.00972.

[53] J. Huang, Y. Yamakawa, R. Tazai, and H. Kontani, Odd-parity intra-unit-cell bond-order and induced nematicity in kagome metal $CsTi_3Bi_5$ driven by quantum interference mechanism, arXiv:2305.18093.